Surface & Coatings Technology 334 (2018) 1–6

Contents lists available at ScienceDirect

Surface & Coatings Technology

journal homepage: www.elsevier.com/locate/surfcoat

Nanocrystalline/amorphous biphase enhanced mechanical properties in multilayer carbon films

Peidong Xue[a,b], Lei Yang[a], Dongfeng Diao[b,*]

[a] Key Laboratory of Education Ministry for Modern Design and Rotor-Bearing System, School of Mechanical Engineering, Xi'an Jiaotong University, Xi'an 710049, China
[b] Institute of Nanosurface Science and Engineering, Guangdong Provincial Key Laboratory of Micro/Nano Optomechatronics Engineering, Shenzhen University, Shenzhen 518060, China

ARTICLE INFO

Keywords:
Multilayer carbon film
Ultrathin single layer
Interface structure
Mechanical properties

ABSTRACT

This study reports the nanostructure evolution and mechanical properties improvement in the nanocrystalline/amorphous multilayer carbon films. Electron cyclotron resonance sputtering and electron/ion alternative irradiation techniques were used to deposit the multilayer carbon films with the total film thicknesses ranging from 130 to 10 nm and the single layer thicknesses ranging from 4 to 1 nm. The high resolution transmission electron microscopy observation showed that the interface between nanocrystalline layer and amorphous layer evolved from an original toothed structure to a mixed biphase structure, and the nanocrystallite size in nanocrystalline layer decreased when layer thickness was reduced from 4 to 1 nm. The nano-indenter tests showed a significant improvement in hardness of multilayer film when single layer thickness was reduced from 4 to 1 nm. The scratch tests revealed that good scratch resistance could be preserved in the multilayer film with 1 nm single layer thickness when total film thickness was only 10 nm. This work may shed light on the ultrathin multilayered coating technology.

1. Introduction

Multilayer technique is by far one of the most versatile methods to assemble multifunctional nanoscale materials with controlled nanometer-scale composition and structure [1]. Among various functional nanoscale objects, carbon-based nanomaterials are promising candidates for emerging science and technology with their unique physical and mechanical properties [2]. It was found that adding the nanocrystallite of fullerenes [3–5], carbon nanotubes [6–8] or graphitic sheets [9] into carbon films could modify certain properties of the original films. Our group recently prepared a kind of graphene sheets embedded carbon film using electron cyclotron resonance (ECR) electron irradiation. This film was proved to have high conductivity [10], paramagnetism [11] and large magnetoresistance [12]. Assembling different hybrid carbon films into multilayer system with convenient PVD or CVD method could further utilize the merits of carbon-based nanomaterials. Based on the various properties of nanocrystalline carbon films, multilayer carbon films could be promising candidates for versatile applications in MEMS/NEMS system.

Various approaches have been made to modulate the properties of carbon-based multilayer films including replacing one component layer with other elements [13], changing deposition parameters [14] and tuning single layer thickness [15–17]. Among these approaches, tuning single layer thickness could preserve the original structures of the component layers while changing the mechanical properties of the multilayer films notably [18], which could bring a method for developing novel functional materials equipped with good mechanical properties. But the ultrathin single layer thickness may bring different changes in mechanical properties in different multilayer system. Some systems would achieve remarkable hardness improvement [19] while others would lose their good mechanical properties [20,21]. And the ultrathin single layer thickness might limit the growth of nanocrystallite within certain component layers, which could influence the crystal structure of the component layers [22,23]. Our former study on nanocrystalline/amorphous multilayer carbon films found that when single layer thickness was reduced from 60 to 5 nm, the nanocrystalline structure was kept intact in the component layers while the hardness increased monotonously [18]. However, when the thickness of single layer was less than 5 nm, the thickness of single layer would reach the same scale as the size of nanocrystallite and interdiffusion effect would be notable. Clarify the influence of the changed nanostructure on the mechanical properties of multilayer film with ultrathin single layer thickness could bring new method for designing novel multifunctional films equipped with good mechanical properties.

* Corresponding author.
E-mail address: dfdiao@szu.edu.cn (D. Diao).

https://doi.org/10.1016/j.surfcoat.2017.10.061
Received 21 June 2017; Received in revised form 18 October 2017; Accepted 23 October 2017
Available online 25 October 2017

In this study, nanocrystalline/amorphous carbon multilayer films with the total film thicknesses ranging from 130 to 10 nm and the single layer thicknesses ranging from 4 to 1 nm were fabricated using ECR sputtering and electron/ion alternative irradiation. The evolution of interface structure, surface roughness and bonding structure of the prepared films were characterized with transmission electron microscopy (TEM), atomic force microscopy (AFM) and Raman spectra, respectively. The hardness and elastic modulus of the carbon multilayer films was evaluated with nano-indentation tests. For further evaluating the mechanical performance of the films with ultrathin total thickness, scratch resistances of multilayer and component films with different total film thicknesses ranging from 130 to 10 nm were evaluated by AFM diamond tip scratch tests.

2. Experiment methods

2.1. Film preparation

Multilayer carbon films composed of alternative electron irradiated layers and ion irradiated layers were deposited on silicon substrate (type 〈100〉) using mirror confinement electron cyclotron resonance (MCECR) and divergence electron cyclotron resonance (DECR) plasma sputtering system, respectively. In MCECR plasma sputtering system, current was applied to two magnetic coils to form a mirror confinement magnetic field. While in DECR plasma sputtering system, current was only applied to one magnetic coil to form a divergence magnetic field. By using different plasma sputtering system, different sputtering energy and density could be obtained [24]. The detailed description of ECR system and the alternative irradiation method were reported in our previous works [10,18]. The substrates with thickness of 0.5 mm were cut into 20 mm × 20 mm square and cleaned in acetone and ethanol bath sequentially by ultrasonic bath before fixed onto the substrate holder. The chamber was first evacuated to a background pressure of 4.00×10^{-4} Pa, then the working pressure was controlled to 4.00×10^{-2} Pa by inflating pure argon gas. The substrates were heated up and kept at 200 °C for an hour to remove the water molecular may exist on the substrate. After cooling down to 80 °C, the substrates were cleaned by argon ion sputtering for 3 min with substrate bias of − 50 V as pretreatment. During the deposition, a DC bias voltage of − 300 V was applied to the round carbon target with a purity of 99.9%. The substrate bias was set as + 100 V during electron irradiated layers deposition and − 5 V during ion irradiated layers deposition, respectively. In the deposition process, one intermediate layer (IL) was firstly deposited with ion irradiation to enhance the adhesion force between the multilayer film and the substrate. Then electron irradiated layers and ion irradiated layers with equivalent thickness were deposited layer by layer to construct the whole multilayer films. The single layer thicknesses were set as 1, 2, 3 and 4 nm. With each certain single layer thickness, multilayer carbon films with total film thicknesses of 130, 90, 50 and 10 nm were deposited. Pure component films were also fabricated for comparison. Multilayer carbon films with single layer thickness of 1, 2, 3 and 4 nm were named as L-1, L-2, L-3 and L-4, respectively. And pure electron irradiated carbon film and ion irradiated carbon film were named as L-E and L-I, respectively. Total film thickness, IL thickness and number of layers of all the multilayer samples are summarized in Table 1.

2.2. Characterization of films

The nanostructures of the carbon films were observed with a Tecnai F30 transmission electron microscope (TEM) operated at 300 kV. The bonding structures of the films were studied by Raman spectra, which were obtained with a HORIBA HR800 laser confocal Raman spectrometer. The 514 nm laser spot size was 2 μm using a 100 × objective, and the spectrum region was between 1100 and 3500 cm^{-1}. The surface morphologies were measured with an Innova atomic force microscope (AFM) which was installed in a glove box filled with Nitrogen. The scanning size was 5 μm × 5 μm and the scanning tip was a silicon tip with tip radius of 2 nm.

The hardnesses of different carbon films and Si substrate were measured by a nanoindenter (Hysitron TI-900) and calculated by Oliver-Pharr method. In the test, a Berkovich diamond indenter with a tip radius of 200 nm was used and the maximum load for indentation was 1 mN. A pre-test on quartz standard sample was done to calibrate the equipment. The values of the elastic modulus and hardness of the samples were given by averaging three different measurement results.

In order to further investigate the mechanical properties of multilayer films with ultrathin total film thickness. Scratch tests were conducted by AFM using a diamond tip with tip radius of 40 nm and the load of scratch was set as 120 μN. The scratch velocity was set as 0.1 μm/s. Each sample was scratched for three times and the scratch depth was given by calculating the average depth.

3. Experiment results

3.1. Nanostructures

Fig. 1(a–c) shows the local TEM cross-sectional images of L-1, L-2 and L-3 with total film thickness of 130 nm. The properly rotated inset figures show the enlarged view of the local structure. The component layer thicknesses for the L-1, L-2 and L-3 were 1 nm, 2 nm and 3 nm and the total thicknesses for all of the three samples were 130 nm, as expected. When single layer thickness was reduced, the layered structure became blurred. However, the sequential bright and dark structure still could be observed even for L-1. The dark layers were deposited with ion irradiation and the bright layers were deposited with electron irradiation.

According to the inset figures, the interface evolution could be observed clearly when the single layer thickness decreased. Influenced by the interface mixing and the interdiffusion effects, the interface between nanocrystalline layer and amorphous layer possessed three different shapes when the single layer thickness was reduced from 3 nm to 1 nm. The interface of L-3 was more like toothed structure as the two component layers intruding into each other. For L-2, owing to the decreased single layer thickness, the protruding tooth like structure connecting the adjacent layers and form a linked-layer structure. For L-1, although the layered structure still could be observed in the whole image, the enlarged local image showed a less identifiable layer structure or biphase structure.

Fig. 1(d–f) shows the typical high resolution transmission electron microscopy (HRTEM) images of L-1, L-2 and L-3. The layered structure could not be observed clearly at this scale owing to the low contrast. The graphene nanocrystallite, which can influence the electrical and

Table 1
Total thicknesses, IL thickness and number of bilayers of the multilayer samples.

Samples	L-4				L-3				L-2				L-1			
Single layer thickness (nm)	4				3				2				1			
Total thickness (nm)	130	90	50	10	130	88	52	8	130	90	50	10	130	90	50	10
IL thickness (nm)	10	10	10	2	10	10	10	2	10	10	10	2	10	10	10	2
Number of layers	30	20	10	2	40	26	14	2	60	40	20	4	120	80	40	8

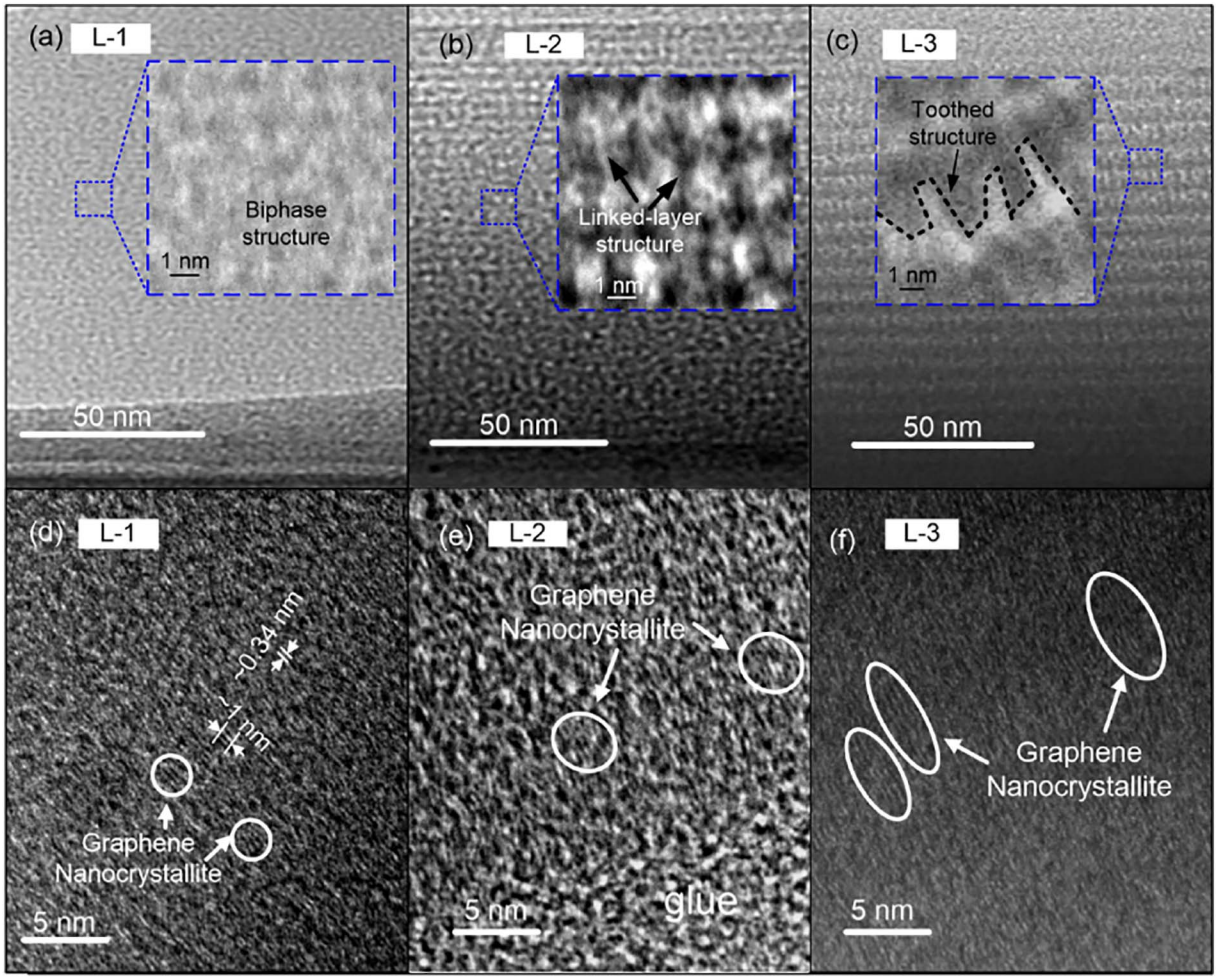

Fig. 1. TEM images of L-1, L-2 and L-3. (a–c) TEM cross-sectional images of the L-1, L-2 and L-3, respectively. The total thickness of 130 nm and bright/dark sequential layers could be observed. An evolution of the interface structure from a toothed structure to a biphase structure could be observed in the inset images. (d–f) HRTEM cross-sectional images of L-1, L-2 and L-3, respectively. It could be observed that the graphene nanocrystallite size decreased with single layer thickness decreasing. The interplanar space is about 0.34 nm and the size of graphene nanocrystallite is about 1 nm as shown.

mechanical properties of the multilayer films, could be observed in all of the three images. According to Fig. 1(d), the interplanar spacing between graphene sheets was approximately 0.34 nm and the orientation of graphene nanocrystallite was perpendicular to the substrate. The size of the graphene nanocrystallite in L-1 was around 1 nm, which should be explained as the alternative deposition of the component layers interrupt the growth of large graphene nanocrystallite in nanocrystalline layers. Similar tendency was also observed in other multilayer systems with ultrathin single layer thickness [23,25].

3.2. Bonding structure

Fig. 2(a) depicts the Raman spectra of L-E, L-I and multilayer carbon films with different single layer thicknesses. The D peak arises due to the presence of sp^2 carbon atoms in rings, while the G peak arises due to the presence of sp^2 carbon atoms in both rings and chains [26–30]. The spectrum of L-I exhibited a composite band centered near 1500 cm^{-1}, which indicated an amorphous structure. While the spectrum of L-E showed separate D and G bands near 1340 cm^{-1} and 1600 cm^{-1}, which indicated an ordered nanocrystalline structure. For the multilayer films, both of the electron and ion irradiated layers contributed to the Raman signal. We have proven that the bonding structure of electron irradiate layers preserved in multilayer films with single layer thickness beyond 5 nm by using a brief difference Raman spectra method [18]. However, when single layer thickness was further

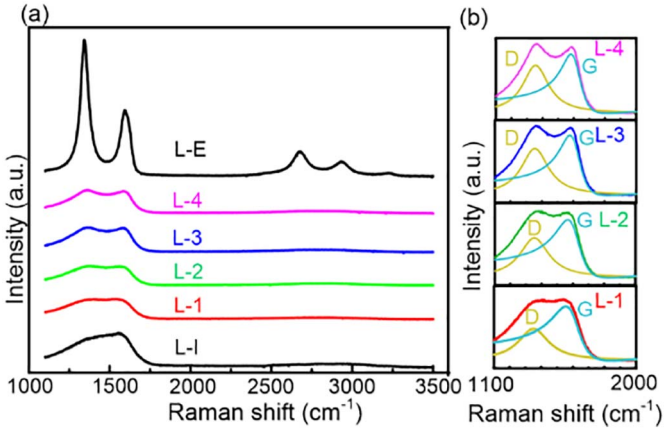

Fig. 2. (a) Raman spectra of different films ranging from 1100 to 3500 cm^{-1}. (b) Raman spectra of different films ranging from 1100 to 2000 cm^{-1}. D peak and G peak become obscure with the decrease of single layer thickness.

reduced to less than 5 nm, the bonding structure exhibited apparent changes that D and G peak became less identifiable. The changing of the Raman spectra could also prove the existence of nanocrystalline structure because the Raman spectra of amorphous multilayer carbon films should not change with the changing of single layer thickness.

Table 2
Raman spectra results of the multilayer carbon films with different single layer thicknesses.

Samples	L-4	L-3	L-2	L-1
G peak positions (cm^{-1})	1582.5	1578.7	1569.2	1555.8
I_D/I_G	0.81	0.78	0.72	0.60

In order to observe the spectra evolution more clearly, Fig. 2(b) depicts the spectra of different samples ranging from 1100 to 2000 cm^{-1} and the decomposed D and G peak. The D band and G band were fitted with a Lorentzian line and a Breit–Wigner–Fano (BWF) line, respectively. The G peak position and the ratio of D peak intensity to G peak intensity (I_D/I_G) were calculated according to the decomposed D and G band [29]. The Raman spectra results were summarized in Table 2. When single layer thickness decreased, the G band position shifted to low frequency and the value of I_D/I_G decreased. The in-plane size of graphene nanocrystallite could be estimated according to the value of I_D/I_G. For multilayer films, the estimation for exact size of the graphene nanocrystallite may not be accurate but we could still conclude a tendency that the in-plane graphene nanocrystallite size would drop when the single layer thickness was reduced.

3.3. Surface roughness

Fig. 3 presents the surface topographies, average roughness (R_a) and root mean square roughness (R_q) values of the multilayer films with different single layer thicknesses. The mean surface roughness of all the multilayer films was around 0.1 nm, which was lower than that of L-E (R_a = 6.78 nm) and L-I (R_a = 0.14 nm). The ultra-smooth surface could make the multilayer films suitable to be applied in MEMS and NEMS.

It is also observed that the multilayer film would be smoother than pure component film in other system [31]. Usually carbon film with high sp^3 would possess relatively smooth surface [32], while the appearance of graphene nanocrystallite within carbon films would lead to high surface roughness [33,34]. For multilayer carbon film with ultrathin single layer thickness, the electron irradiated nanocrystalline layers were too thin to grow high asperities. When one layer nanocrystalline layer was deposited, the following ion irradiated amorphous layer could break the growth of nanocrystallite, and the low energy ion bombardment during the deposition would help smooth the surface [35,36]. Thus, each new deposited layer could grow on a smooth surface and a thick film with smooth surface could be formed as a result.

3.4. Mechanical behaviors

Fig. 4(a) shows the load-displacement curves of multilayer films with total thickness of 130 nm during the indentation. Fig. 4(b) summarizes the hardness value as a function of single layer thickness. Some data were extracted from our former work for better comparison, which were marked with hollow symbols [18]. As the total thickness of those samples were 130 nm, the maximum penetration depth of the indenter went beyond 20% of the film thickness, which means the values of the hardness were partly influenced by the substrate [37,38]. Because the hardness of the Si substrate was 11.5 ± 0.3 GPa, L-1 and L-2 should be considered as hard films on soft substrate, while L-3 and L-4 should be considered as soft films on hard substrate [39]. Thus, the real hardness values of L-1 and L-2 should be slightly larger than the presented values, while the real hardness values of L-3 and L-4 should be slightly smaller than the presented values. According to Fig. 4(b), when single layer thickness decreased, the hardness of the multilayer films increased monotonously. Compared with the slow increase in hardness when single layer thickness decreased from 60 to 10 nm, the hardness increased nearly 70% when single layer thickness decreased from 4 to 1 nm. The hardness of L-1 was 17.1 GPa, which was even higher than that of the pure hard component film L-I with a hardness value of 13.1 GPa. Reasons for the abnormal hardness increasing rate should be highly related to the nanostructure changes and we will discuss it later. Fig. 4(c) presents the elastic modulus of different samples as a function of single layer thickness. The value of elastic modulus exhibited the same tendency as hardness. Fig. 4(d) presents the plastic resistance parameter (H/E), which was found to be an important parameter to estimate both elastic-plastic behavior of thin film and provide information about wear resistance. The H/E ratio shows the physical response of an atomic lattice to an external force and relates to the bulk fracture strength [40]. The H/E ratio also increased when single layer thickness decreased. Interestingly, the H/E ratio of L-1 was slightly larger than 0.1, which should vary in the range between 0 and 0.1 for DLC. This high H/E value of L-1 might be attributed to the biphase structure of the multilayer films and implied a high wear resistance.

3.5. Scratch resistance

Fig. 5 presents the cross-sectional topographies across the scratches (as shown in the inset figures) on the surface of L-1 and L-4. The scratch depth of L-1 was 1.1 nm while the scratch depth of L-4 was 4.2 nm. Considering the multilayer films were very smooth, the scratch process

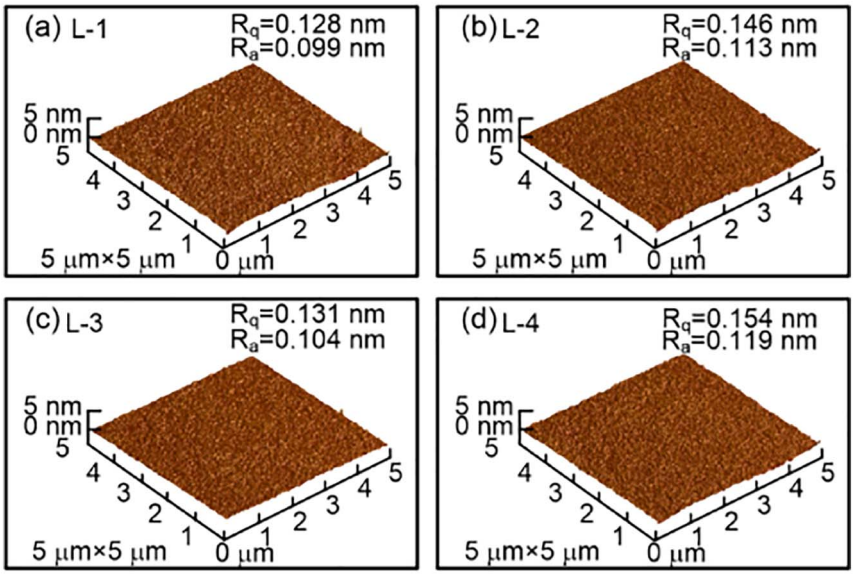

Fig. 3. AFM images of different multilayer carbon films. All films possess smooth surface.

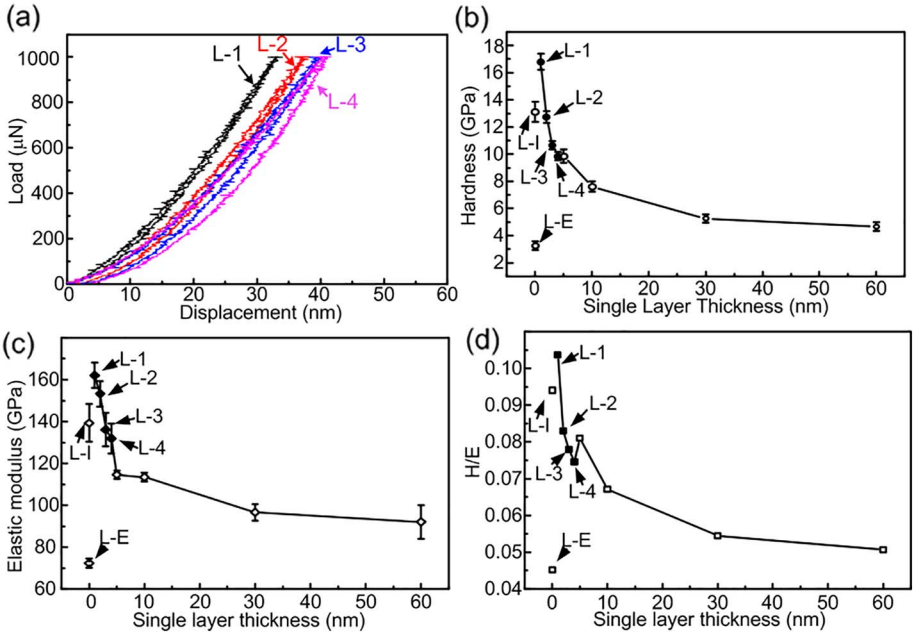

Fig. 4. (a) Load-displacement curves of L-1 to L-4. (b) Hardness as a function of single layer thickness. (c) Elastic modulus as a function of single layer thickness. (d) H/E as a function of single layer thickness.

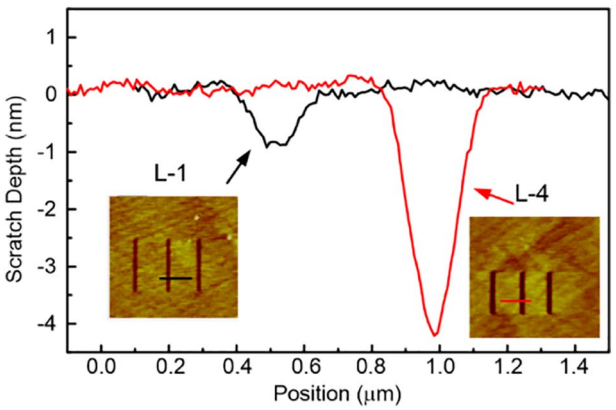

Fig. 5. Cross-sectional topographies across the scratches of L-1 and L-4. The inset images present the AFM image of the scratch areas.

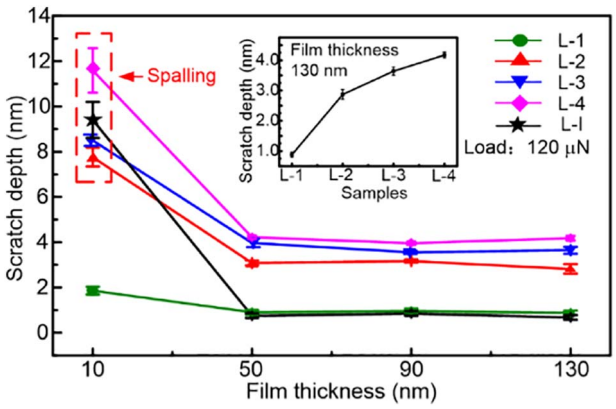

Fig. 6. Scratch depth of L-I and different multilayer films with different total thicknesses. L-1 could preserve good scratch resistance when the film total thickness was reduced to 10 nm. The inset figure shows the scratch depth of different multilayer carbon film with total thickness of 130 nm.

could be equivalent to the wear process that an asperity scratch on a plane. Thus, the shallow scratch depth of L-1 could be explained by both of the high hardness and the high H/E ratio.

Fig. 6 summarizes the scratch depth of different samples with different total thicknesses under the same load. The inset figure shows the scratch depth of different multilayer carbon films with total film thickness of 130 nm. Single layer thickness decreasing would improve the scratch resistance notably. And although the hardness value of L-1 and L-I were different, their scratch resistance capability were nearly the same. It could be concluded that when the total thicknesses of the films were beyond 50 nm, the scratch resistance of the multilayer films did not change notably. However, when total film thickness was reduced to 10 nm, the scratch depth of L-2, L-3 and L-4 sudden rose to 7.8, 8.5 nm and 11.5 nm, respectively. The sudden rise in scratch depth means these multilayer films spalled under this normal load. This could be explained that when the total film thickness was decreased to 10 nm, the scratch depth was more than 20% of the total thickness, the scratch resistance would be influenced by the substrate. For L-I and L-1, the scratch depth was nearly the same when the total thickness of the films larger than 50 nm. When total film thickness was reduced to 10 nm, the scratch depth of L-I increased to nearly 10 nm while L-1 still kept a good scratch resistance. For pure carbon films, the mechanical properties of an ultra-thin film are softer than what expected for the same film if it was thick. The softening of the mechanical properties of ultrathin films is a size effect [41,42]. But for the multilayer film with ultrathin component layers, it could still keep a high interfaces amount with ultrathin total thickness and keep a good scratch resistance as a result.

4. Discussions

In this work, we found that when the single layer thickness of nanocrystalline/amorphous multilayer carbon film decreased from 4 to 1 nm, the interface structure of the multilayer films evolved from a toothed structure to a biphase structure and the nanocrystallite size decreased at the same time. The decreased single layer thickness also brought a significant hardness improvement in the multilayer films. The formation of coherent interface, the biphase structure and the decreased nanocrystallite size were considered as the factors influencing the hardness.

In the first place, during the electron irradiated layer deposition, the electron could penetrate in the former deposited ion irradiated layer when the thickness of single layer was thin enough [43]. The penetrating electron may induce the former deposited amorphous ion irradiated layer to form some graphene nanocrystallites [43]. When

graphene nanocrystallite existed in both of the two phases, a coherent interface could form between the electron and ion irradiated phases. The formation of the coherent interface was considered to result in hardness increase [44]. Second, when the biphase structure formed in the multilayer films, the interfaces between electron irradiated phases and ion irradiated phases increased remarkably. Considering the two phases possessed large difference in modulus, the interfaces could block the movement of dislocation in the film efficiently [45,46]. Third, when single layer thickness was reduced below 3 nm, the graphene nanocrystallite size in the electron irradiated phases also decreased as a consequence. The decreased graphene nanocrystallite could improve the strength of nanocrystalline phase, which was known as the Hall-Petch effect [47,48]. The strength improvement of one phase could benefit in enhancing the total hardness [14]. As a result, a significant hardness improvement was achieved in the multilayer films when single layer thickness became ultrathin.

5. Conclusion

In this study, we used the electron/ion alternative irradiation technology in ECR sputtering system to deposit multilayer carbon films. We studied the nanostructure evolution and the mechanical properties improvement induced by the change of single layer thickness (4 to 1 nm). The evolution of interface structure from a toothed structure to a biphase structure was observed by HRTEM images. The decrease of graphene nanocrystallite size was verified by both HRTEM images and Raman spectra. Very smooth surface (Ra around 0.1 nm) could be obtained for multilayer carbon film with ultrathin single component layers. According to the indentation test, prominent improvements in hardness, elastic modulus and H/E were observed when single layer thickness was reduced from 4 to 1 nm. According to the scratch test, when the total film thickness was reduced from 130 to 10 nm, good scratch resistance was kept in the multilayer film with single layer thickness of 1 nm. The hardness improvement was attributed to the coherent interface, biphase structure and small nanocrystallite size. This work may be useful for designing ultrathin protective multilayer films.

Acknowledgements

The authors would like to thank the National Natural Science Foundation of China under Grant No. of 51575359 and 51605369, China Postdoctoral Science Foundation under Grant No. of 2015M572547. Shenzhen Fundamental Research subject-layout project (JCYJ20160427105015701).

References

[1] F. Caruso, R.A. Caruso, H. Möhwald, Nanoengineering of inorganic and hybrid hollow spheres by colloidal templating, Science 282 (1998) 1111–1114.
[2] J. Hong, J.Y. Han, H. Yoon, et al., Carbon-based layer-by-layer nanostructures: from films to hollow capsules, Nano 3 (2011) 4515–4531.
[3] Q. Wang, C. Wang, Z. Wang, et al., Fullerene nanostructure-induced excellent mechanical properties in hydrogenated amorphous carbon, Appl. Phys. Lett. 91 (2007) 141902.
[4] I. Alexandrou, H.J. Scheibe, C.J. Kiely, et al., Carbon films with a sp 2 network structure, Phys. Rev. B. 60 (1999) 10903.
[5] Z. Wang, C.B. Wang, B. Zhang, et al., Ultralow friction behaviors of hydrogenated fullerene-like carbon films: effect of normal load and surface tribochemistry, Tribol. Lett. 41 (2011) 607–615.
[6] H. Zanin, P.W. May, M. Hamanaka, et al., Field emission from hybrid diamond-like carbon and carbon nanotube composite structures, ACS Appl. Mater. Interfaces 5 (2013) 12238–12243.
[7] M.G. Fyta, P.C. Kelires, Simulations of composite carbon films with nanotube inclusions, Appl. Phys. Lett. 86 (2005) 191916.
[8] L. Li, J.B. Niu, Z.H. Xia, et al., Nanotube/matrix interfacial friction and sliding in composites with an amorphous carbon matrix, Scr. Mater. 65 (2011) 1014–1017.
[9] M. Shakerzadeh, G.C. Loh, N. Xu, et al., Re-ordering chaotic carbon: origins and application of textured carbon, Adv. Mater. 24 (2012) 4112–4123.
[10] C. Wang, D.F. Diao, X. Fan, C. Chen, Graphene sheets embedded carbon film prepared by electron irradiation in electron cyclotron resonance plasma, Appl. Phys. Lett. 100 (2012) 231909.
[11] C. Wang, D.F. Diao, Magnetic behavior of graphene sheets embedded carbon film originated from graphene nanocrystallite, Appl. Phys. Lett. 102 (2013) 052402.
[12] C. Wang, D.F. Diao, Self-magnetism induced large magnetoresistance at room temperature region in graphene nanocrystallited carbon film, Carbon 112 (2017) 162–168.
[13] N. Dwivedi, C. Dhand, I. Rawal, et al., Anomalous electron transport in metal/carbon multijunction devices by engineering of the carbon thickness and selecting metal layer, J. Appl. Phys. 121 (2017) 225101.
[14] Y. Zhang, Y. Zhai, F. Li, et al., Effect of microstructure and mechanical properties difference between sub-layers on the performance of alternate hard and soft diamond-like carbon multilayer films, Surf. Coat. Technol. 232 (2013) 575–581.
[15] S. Logothetidis, C. Charitidis, M. Gioti, et al., Comprehensive study on the properties of multilayered amorphous carbon films, Diam. Relat. Mater. 9 (2000) 756–760.
[16] S. Logothetidis, S. Kassavetis, C. Charitidis, et al., Nanoindentation studies of multilayer amorphous carbon films, Carbon 42 (2004) 1133–1136.
[17] C. Mathioudakis, P.C. Kelires, Y. Panagiotatos, et al., Nanomechanical properties of multilayered amorphous carbon structures, Phys. Rev. B 65 (2002) 205203.
[18] P. Xue, L. Yang, D. Diao, ECR sputtering and electron/ion alternative irradiation for multilayer carbon films fabrication with tunable layer thickness, Surf. Coat. Technol. 296 (2016) 26–32.
[19] S. Vepřek, S. Reiprich, L. Shizhi, Superhard nanocrystalline composite materials: the TiN/Si3N4 system, Appl. Phys. Lett. 66 (1995) 2640–2642.
[20] P.B. Mirkarimi, L. Hultman, S.A. Barnett, Enhanced hardness in lattice-matched single-crystal TiN/V0. 6Nb0. 4N superlattices, Appl. Phys. Lett. 57 (1990) 2654–2656.
[21] J. Xu, M. Kamiko, Y. Zhou, et al., Structure transformations and superhardness effects in V/Ti nanostructured multilayers, Appl. Phys. Lett. 81 (2002) 1189–1191.
[22] W. Li, P. Liu, Y. Zhao, et al., New understanding of hardening mechanism of TiN/SiN x-based nanocomposite films, Nanoscale Res. Lett. 8 (2013) 1–7.
[23] Z.J. Liu, Y.G. Shen, Effects of amorphous matrix on the grain growth kinetics in two-phase nanostructured films: a Monte Carlo study, Acta Mater. 52 (2004) 729–736.
[24] X. Fan, D. Diao, K. Wang, et al., Multi-functional ECR plasma sputtering system for preparing amorphous carbon and Al–O–Si films, Surf. Coat. Technol. 206 (2011) 1963–1970.
[25] E. Rismani, R. Yeo, H. Mirabolghasemi, et al., An ultrathin multilayer TiN/SiN wear resistant coating for advanced magnetic tape drive heads, Thin Solid Films 556 (2014) 354–360.
[26] F. Rose, N. Wang, R. Smith, et al., Complete characterization by Raman spectroscopy of the structural properties of thin hydrogenated diamond-like carbon films exposed to rapid thermal annealing, J. Appl. Phys. 116 (2014) 123516.
[27] C. Casiraghi, A.C. Ferrari, J. Robertson, et al., Ultra-thin carbon layer for high density magnetic storage devices, Diam. Relat. Mater. 13 (2004) 1480–1485.
[28] A.C. Ferrari, J. Robertson, Resonant Raman spectroscopy of disordered, amorphous, and diamondlike carbon, Phys. Rev. B 64 (2001) 075414.
[29] A.C. Ferrari, J. Robertson, Interpretation of Raman spectra of disordered and amorphous carbon, Phys. Rev. B 61 (2000) 14095–14107.
[30] N. Dwivedi, S. Kumar, J.D. Carey, et al., Photoconductivity and characterization of nitrogen incorporated hydrogenated amorphous carbon thin films, J. Appl. Phys. 112 (2012) 113706.
[31] Y.Y. Tse, D. Babonneau, A. Michel, et al., Nanometer-scale multilayer coatings combining a soft metallic phase and a hard nitride phase: study of the interface structure and morphology, Surf. Coat. Technol. 180 (2004) 470–477.
[32] T. Yoshitake, T. Nishiyama, H. Aoki, et al., Atomic force microscope study of carbon thin films prepared by pulsed laser deposition, Appl. Surf. Sci. 141 (1999) 129–137.
[33] O.V. Penkov, V.E. Pukha, E.N. Zubarev, et al., Tribological properties of nanostructured DLC coatings deposited by C 60 ion beam, Tribol. Int. 60 (2013) 127–135.
[34] C. Chen, D. Diao, X. Fan, et al., Frictional behavior of carbon film embedded with controlling-sized graphene nanocrystallites, Tribol. Lett. 55 (2014) 429–435.
[35] E. Chason, T.M. Mayer, Low energy ion bombardment induced roughening and smoothing of SiO2 surfaces, Appl. Phys. Lett. 62 (1993) 363–365.
[36] D. Diao, C. Wang, X. Fan, Frictional behavior of nanostructured carbon films, Friction 1 (2013) 63–71.
[37] B. Jönsson, S. Hogmark, Hardness measurements of thin films, Thin Solid Films 114 (1984) 257–269.
[38] B. Bhushan, Chemical, mechanical and tribological characterization of ultra-thin and hard amorphous carbon coatings as thin as 3.5 nm: recent developments, Diam. Relat. Mater. 8 (1999) 1985–2015.
[39] G.M. Pharr, W.C. Oliver, Measurement of thin film mechanical properties using nanoindentation, MRS Bull. 17 (1992) 28–33.
[40] N. Dwivedi, S. Kumar, H.K. Malik, Nanoindentation measurements on modified diamond-like carbon thin films, Appl. Surf. Sci. 257 (2011) 9953–9959.
[41] A.C. Ferrari, Diamond-like carbon for magnetic storage disks, Surf. Coat. Technol. 180 (2004) 190–206.
[42] N. Dwivedi, R.J. Yeo, Z. Zhang, et al., Direct observation of thickness and foreign interlayer driven abrupt structural transformation in ultrathin carbon and hybrid silicon nitride/carbon films, Carbon 115 (2017) 701–719.
[43] C. Chen, X. Fan, D. Diao, Low-energy electron irradiation induced top-surface nanocrystallization of amorphous carbon film, Appl. Surf. Sci. 384 (2016) 341–347.
[44] X. Hu, H. Zhang, J. Dai, et al., Study on the superhardness mechanism of Ti–Si–N nanocomposite films: influence of the thickness of the Si 3 N 4 interfacial phase, J. Vac. Sci. Technol., A 23 (2005) 114–117.
[45] J.S. Koehler, Attempt to design a strong solid, Phys. Rev. B 2 (1970) 547.
[46] G. Abadias, S. Dub, R. Shmegera, Nanoindentation hardness and structure of ion beam sputtered TiN, W and TiN/W multilayer hard coatings, Surf. Coat. Technol. 200 (2006) 6538–6543.
[47] E.O. Hall, The deformation and ageing of mild steel: III discussion of results, Proc. Phys. Soc. Lond. B 64 (1951) 747–753.
[48] N.J. Petch, The cleavage of polycrystals, J. Iron Steel Inst. 174 (1953) 25–28.